Mechanism of HflX-mediated recycling of *E. coli* ribosome studied by time-resolved cryo-EM

Sayan Bhattacharjee[1,#], Xiangsong Feng[1,#], Suvrajit Maji[1], Zuben P Brown[1,2], Joachim Frank[1*].

[1]Biochemistry and Molecular Biophysics & Biological Sciences, Columbia University, New York, USA
[2] Current address: Thermo Fisher Scientific, Oregon, USA
[#] These authors contributed equally
* Corresponding author

Recycling of stalled, translationally inactive ribosomes is one of the response mechanisms underlying resistance to environmental stress. HflX, a bacterial GTPase overexpressed upon heat shock and exposure to antibiotics, catalyzes the splitting of stalled ribosomes[1-6]. Due to its rapid rate, an attempt to follow this process in real time at room temperature requires time-resolved techniques on the scale of tens of milliseconds[1]. Here we show the time course of the splitting of *E. coli* 70S ribosome by HflX in the presence of GTP using time-resolved cryo-EM with a microfluidic device. We report the structures of three short-lived intermediate states within 140 ms of mixing 70S ribosomes with HflX and GTP. Binding of HflX and GTP hydrolysis induces breakage of multiple intersubunit bridges and opening of the 70S ribosome in a clamshell-like manner as the 30S subunit rotates around an axis with hinges formed by the remaining intersubunit bridges B3 and B7a. At 900 ms virtually all ribosomes are dissociated, while HflX remains bound to the 50S subunit. Our analysis of the structural intermediates not only allows the mechanism of HflX-catalyzed ribosome splitting to be followed in molecular detail but also to shed light on related processes: recycling of the post-termination complex by RRF/EF-G.

39 In *Escherichia coli* (*E. coli*), GTPase ***H**igh **f**requency of **l**ysogenization **X***
40 (HflX), a universally conserved protein for prokaryotes, acts as a ribosome-
41 splitting factor during the heat shock response[1,6,7]. Recent studies revealed that
42 HflX splits antibiotic-stalled 70S ribosomes from pathogenic *Mycobacterium*
43 *abscessus* and nonpathogenic *Mycobacterium smegmatis*[3], dissociates
44 hibernating homodimeric 70S into 50S and 30S subunits in *Staphylococcus*
45 *aureus*[8], regulates hypoxia-induced replication arrest in *Mycobacterium bovis*[2],
46 binds to the 50S subunit of *Chlamydophila pneumoniae*[5] and *Sulfolobus*
47 *solfataricus*[9], and acts as a gatekeeper by regulating the manganese level in *E.*
48 *coli*[4]. Thus, HflX is a remarkably multi-functional protein with a common
49 mode of action: the splitting of stalled 70S ribosomes into its subunits in a wide
50 range of prokaryotes. Given that HflX shares structural similarities with
51 Release Factors 3 (RF3) and Ribosome Recycling Factor (RRF) on the
52 ribosome and that it occupies the A-site tRNA position on the 50S subunit
53 similar to the release factor's GGQ motif–containing loop[1], the time-dependent
54 structural study on the progressive splitting of the 70S by HflX could reveal
55 the mechanism of ribosome recycling, as well. Furthemore understanding the
56 detailed structural mechanism of splitting could benefit the development of a
57 new class of broad-spectrum antibiotics.

58 *E. coli* HflX consists of four domains: N-terminal domain (NTD), GTP
59 binding domain (GBD), C-terminal domain (CTD), and helical linker domain
60 (HLD)[1,10]. The cryo-EM structure of the HflX-50S complex in the presence of
61 GMP-PNP, a non-hydrolysable GTP analog, reveals that the HLD and NTD of
62 HflX bind to the peptidyl transferase center in a way similar to RRF, causing
63 significant conformational changes in the intersubunit bridge B2a (h44:H69),

64 and thereby promoting the dissociation of the 70S ribosome[1]. According to the
65 dissociation kinetics measured by light scattering, the rate of dissociation of
66 vacant ribosomes (without tRNA and mRNA) by HflX in the presence of
67 GMP-PNP or GTP is $k_{obs\ HflX\text{-}GMP\text{-}PNP} = 0.22 \pm 0.003\ s^{-1}$ and $k_{obs\ GTP} = 0.2 \pm$
68 $0.002\ s^{-1}$, respectively[1]. This rapid rate makes the progress of ribosome
69 splitting by HflX difficult to study at room temperature using the conventional
70 blotting method of cryo-EM sample preparation[11]. So far, the only HflX-bound
71 ribosome structure is the 50S-GNP-PNP complex, which was solved at a
72 resolution of 4.5 Å and considered to represent the state immediately after
73 subunit dissociation[1]. Thus, due to the absence of any structures of short-lived
74 reaction intermediates the mechanism of HflX-mediated ribosome splitting has
75 remained unknown. To capture on-pathway intermediates in an in vitro
76 reaction of HflX-GTP with 70S ribosomes, we used time-resolved cryo-EM[12-
77 16]. We were able to capture three intermediate states, which allowed us to
78 follow the recycling process of 70S ribosomes catalyzed by HflX at room
79 temperature.

80 HflX acts on the 70S ribosome in a nucleotide-dependent way, and light
81 scattering analysis revealed that the rate of ribosome splitting by HflX-GTP
82 (with GTP and RRF-EF-G-GTP the rates are $k_{obs\ HflX\text{-}GTP} = 0.002\ s^{-1}$ and k_{obs}
83 $_{RRF\text{-}EF\text{-}G\text{-}GTP} = 0.005\ s^{-1}$, respectively[6,17]) is very similar to the rate of ribosome
84 dissociation by the combined action of RRF and EF-G-GTP[6,17]. The fraction
85 of ribosomes split into subunits at room temperature within a reaction time of
86 140 ms is close to 50%, according to our earlier TR cryo-EM experiment on
87 *E. coli* ribosome recycling in the presence of RRF, EF-G, and GTP[15]. In view
88 of these findings, we aimed our TR cryo-EM study at a 140 ms reaction time

89 and added both shorter (10 ms and 25 ms) time points and one longer one (900
90 ms) toward the reaction's completion. We mixed 70S ribosomes with the HflX-
91 GTP complex in our mixing-spraying TR cryo-EM apparatus using different
92 PDMS-based microfluidic chips (Methods and Extended Data Fig. 2). As in
93 our previous TR studies[15,16], 3D classification was performed on the entire,
94 pooled dataset. The 3D classification produced seven distinct classes, which
95 we characterized by examination of the corresponding reconstructed density
96 maps. (Here "rotated" and "nonrotated" refers to the presence or absence of
97 intersubunit rotation[18]): (1) rotated 70S without HflX ($r70S_{noHflX}$); (2) non-
98 rotated 70S without HflX ($nr70S_{noHflX}$); (3) 70S-like intermediate-I with HflX
99 ($i70S_{HflX}$-I); (4) 70S like-intermediate-II with HflX ($i70S_{HflX}$-II); (5) 70S-like
100 intermediate-III with HflX ($i70S_{HflX}$-III); (6) 50S with HflX ($50S_{HflX}$); and (7)
101 30S (Methods and Extended Data Fig. 5, and 6). The splitting reaction kinetics
102 of the 70S ribosome, as evaluated by following the number of particles
103 obtained upon 3D classifications from 10 ms to 900 ms, is found to follow a
104 similar roughly exponential behavior as reported from dissociation kinetics
105 measured by light scattering[1] (Fig 1G). Furthermore, we noticed a rapid
106 increase in the number of free 30S particles from 140 ms to 900 ms, which
107 implies that the final separation of the subunits commences not earlier than
108 with state $i70S_{HflX}$-III (Fig. 1G).

109 The three HflX-containing intermediates and $50S_{HflX}$ -- four of the seven
110 3D classes we found -- were selected for additional structural analysis
111 (Methods and Extended Data Fig. 5, and 6A-E). Furthermore, focused 3D
112 classification and subsequent reconstruction of HflX binding regions from
113 each of the resulting class reconstructions yielded high-resolution density maps

114 for four states of HflX: (1) HflX-I, (2) HflX-II, (3) HflX-III, and (4) HflX-IV
115 (Extended Data Fig. 5). Refinement on the three i70S$_{HflX}$ class reconstructions
116 yielded high-resolution on-pathway intermediates i70S$_{HflX}$-I, i70S$_{HflX}$-II, and
117 i70S$_{HflX}$-III (resolutions are indicated in Extended Data Fig. 7 and Extended
118 Data Table 2). The kinetics of the reaction can be followed from the histogram
119 of particle counts in the respective classes (Fig. 1G). Intermediates i70S$_{HflX}$-I,
120 i70S$_{HflX}$-II, and i70S$_{HflX}$-III are each dominated by contributions from 10 ms,
121 25 ms, and 140 ms, respectively. Comparison of the atomic models obtained
122 for these intermediates with one another and with the apo-70S revealed that the
123 opening and splitting of the 70S ribosome occurs in the following steps:
124 First, the ribosome opens slightly to accommodate the initial binding of
125 HflX in i70S$_{HflX}$-I (Fig. 1A). Using the tool previously developed[19] we find
126 that in this first intermediate, the 30S subunit has rotated by 5.9° around an
127 axis (Axis I) that passes through the intersubunit bridges B1b, B2a, B3, and B4
128 (Extended Data Fig. 8A, D, G, and 8J-K), and this rotation has moved protein
129 S6 of 30S into close vicinity to protein L2 of 50S (Fig. 1E-F). Apparently, the
130 insertion of HflX along with the prying apart of the 70S ribosome and the
131 rotation of the 30S subunit are facilitated by the increased backbone entropy
132 of L2 in i70S$_{HflX}$-I compared to apo-70S (the predicted binding and solvation
133 free energies between L2 and S6 are same for apo-70S and i70S$_{HflX}$-I; see
134 Methods and Extended Data Table 3) since we find indication of disorder: the
135 density of L2 is not resolved well in i70S$_{HflX}$-I (Fig. 1F) compared to all its
136 other manifestations in apo-70S, i70S$_{HflX}$-II and i70S$_{HflX}$-III (Fig. 1E, and 2D-
137 F). Comparison of the 50S subunit in i70S$_{HflX}$-I and apo-70S shows that H69
138 has moved by 6.7 Å, apparently by a push by HflX since fitting the model of

139 HflX to apo-70S reveals a steric clash with H69 (Fig. 1H, I). In i70S$_{HflX}$-I HflX
140 is blurred, indicating motion-induced heterogeneity (Extended Data Fig. 5).
141 Going from this first intermediate to i70SHflX-II and i70SHflX-III we
142 observe stepwise rotations, by 7.9° and 8.2°, respectively, of the 30S subunit
143 around a new axis (Axis II) passing through intersubunit bridges B3 and B7a,
144 which are both located along helix h44 (Fig. 1B-C, and Extended Data Fig.
145 8B-C, 8E-F, 8H-I, and 8J-K). In the first step of rotation around this new axis,
146 protein S6 of the 30S subunit moves away from protein L2 (Fig. 2A-B, 2D-E,
147 and Extended Data Fig. 8B, 8E, 8H, and 8J-K). This movement is enabled by
148 a 6.5 Å pull of C1965 of H71 by the loop-helix motif (G74-V100) of HflX
149 NTD (Fig. 3C, and Extended Data Fig. 9A-C). As a consequence bridge B3
150 (h44:H71) as well as bridges B7b and B7bR have become unstable (binding
151 and solvation free energies between L2 and S6 of i70S$_{HflX}$-II decrease from
152 corresponding apo-70S, see Extended Data Table 3). While the conformation
153 of the 30S subunit remains the same from apo-70S to first intermediate, the
154 change from first to second intermediate is accompanied by a rotation of the
155 30S subunit head by 2.1° around another axis, Axis III (Extended Figure 10A-
156 C).
157 In the second step of the 30S subunit rotation around Axis II, from
158 i70S$_{HflX}$-II to i70S$_{HflX}$-III, protein S6 has continued to move away from protein
159 L2 (Fig. 2B-C, 2E-F, and Extended Data Fig. 8C, 8F, 8I, and 8J-K). Bridges
160 B7b and B7bR are now entirely disrupted (no contacts found between L2 and
161 S6 in free energy prediction, see Extended Data Table 3), allowing the flexible
162 loop (E323-G349) of HflX's GTD to readily access the small subunit protein

163 S12, thus positioned to jettison the 30S subunit from the 70S ribosome (Fig.
164 3D).

165 Finally, the reconstruction of the stable 50S-HflX complex, at 3.6 Å
166 resolution (Extended Data Fig. 11A), shows no longer any trace of density
167 from the 30S subunit (Fig. 1D, 3A-B and Extended Data Fig. 11A, and D). This
168 class mainly contains particles from 900 ms (Fig. 1G). The map agrees very
169 well with the map of HflX-50S-GNP-PNP previously published[1] (Extended
170 Data Fig. 11A-C).

171 Comparison of the atomic models built for the three intermediate states
172 reveals that HflX undergoes considerable conformational and positional
173 changes on the 70S ribosome, specifically in its CTD, HLD, and NTD (see
174 movie 1 in Supplementary Material). The domain movements associated with
175 the CTD and HLD match quite well with the dynamics of apo-HflX predicted
176 from 1000 ns of molecular dynamics simulations (Extended Data Fig. 12A-C).
177 Interestingly, the loop-helix motif (G74-V100) of NTD makes stable contact
178 with H71 of the 50S subunit in state HflX-II (Fig. 3C, and Extended Data Fig.
179 9E-G).

180 In trying to understand the actions of HflX, we investigated the
181 nucleotide state of GTP in the different states of HflX. At 25 ms, with
182 exception of their NTDs, the densities of HflX in states HflX-I, HflX-II and
183 associated GTPs are not resolved as well as they are for the other two classes,
184 indicating mobility and preventing determination of nucleotide state (Extended
185 Data Fig. 5). In an attempt to fit the atomic model of GTP to the corresponding
186 densities in HflX-III and HflX-IV, we observed that the density in the region
187 of the nucleotide site on HflX-III is a better fit for GDP·Pi than GTP or GDP

188 (Extended Data Fig. 9A-B) A similar matching effort resulted in a decent
189 match of GTP to the density of HflX bound to the 50S subunit, even though
190 the GDP state is expected to be found at this stage (Extended Data Fig. 9C-D).
191 Since at the 140 ms time point Pi is still associated with GDP and none
192 of the 30S subunits have been cleaved, we conclude that the energy for the
193 breaking of bridges B3 and B7a and the final dissociation of the 30S subunit is
194 set free by Pi release. It is unclear without further investigation if GTP
195 hydrolysis plays a role in the initial stages of splitting, from intermediate I to
196 III, since it is known that HflX can perform the splitting in the absence of GTP,
197 albeit with a slower rate[1]. The likely explanation for the observation of GTP
198 on the 50S subunit-bound HflX molecule at 900 ms is that by that time both Pi
199 and GDP have left and that a new GTP molecule has taken their place
200 (Extended Data Fig. 9C-D).
201 With the axes and angles of 30S subunit rotation known, as well as the
202 location of bridges relative to the axes, we were able to determine the distances
203 between constituent residues of all intersubunit bridges. From these distances
204 we can determine at which time points the intersubunit bridges are ruptured.
205 According to these geometric calculations, the bridges B1a, B1b, B2a, and B2b
206 are already broken at 10 ms. B5, B6 and B7b break within 140 ms. Finally, the
207 last two bridges B3 and B7a, which formed the hinges of Axis II, give way
208 between 140 ms and 900 ms. Bridge B4 (H34:S15) presents an interesting case
209 as it behaves like a spring: its 50S constituent H34 is initially compressed in
210 the step from apo-70S to i70SHflX-I, as HflX is accommodated within the first
211 10 ms, but in the next two steps (10 ms to 25 ms to 140 ms) it is extended. This

212 bridge finally breaks along with B3 and B7a after 140 ms (Extended Data Fig.
213 9H-I).

214 Our study leaves open the question on how HflX recognizes the stalled
215 state of the ribosome. Here our observation of 30S subunit head rotation from
216 apo-70S to i70SHflX-I may offer a clue. Puromysine-treated polysomes,
217 having deacylated tRNA in the P site, display greatly enhanced HflX splitting
218 activity, and this state was proposed as the natural substrate for HflX[1]. In this
219 state, the ribosome is known to undergo spontaneous intersubunit rotation[20]
220 which goes hand in hand with 30S subunit head 'swivel' rotation[21]. This would
221 suggest that HflX initially binds to the ribosome in its rotated conformation
222 and forces it into the unrotated conformation observed in i70SHflX-I, with
223 residual 30S subunit head rotation.

224 Another interesting question is whether our findings about the time
225 course and stepwise process of HflX-catalyzed ribosome splitting may inform
226 us about the time course of RRF/EF-G-GTP-induced splitting of the post-
227 termination complex. (A previous TR cryo-EM study of this process in vitro
228 by our group[15] was unable to observe early states of subunit separation). We
229 see two striking similarities between the two processes: (1) in RRF-bound post-
230 termination complex[15,22], the helix-loop-helix motif of domain I approaches
231 helix 71 within 140 ms, in a position that is similar to the position of the loop-
232 helix motif (G74-V100) of NTD of HflX in intermediate i70S$_{HflX}$-II, similarly
233 capable of pulling on H71 (Extended Data Fig. 9A-C and 10D-G). (2) The final
234 dissociation of the 30S subunit occurs through an interaction of RRF domain
235 II with protein S12, at the expense of hydrolysis of GTP associated with EF-
236 G, in a way that is quite similar to that of the flexible loop (E323-G349) of

237 HflX GTD (Extended Data Fig. 10D-G). (3) A third similarity holds if our
238 hypothesis of HflX binding to the rotated ribosome is correct since the latter is
239 the substrate of RRF/EF-G-GTP binding, as well[23,24].

240 Here, we have shown how time-resolved cryo-EM can capture high-
241 resolution structures of intermediates on-the-fly to reveal short-lived reaction
242 intermediates that represent snapshots of an unfolding molecular mechanism.
243 A combination of experimental and theoretical approaches has been used to
244 study the molecular mechanism of bacterial resistance under stress. Based on
245 our cumulative observations from the examination of the three intermediates,
246 we propose that within 10 ms, the initial binding of HflX is followed by the
247 stepwise clamshell-like opening of the ribosome around an axis that closely
248 aligns with helix 44 of the 30S subunit. By the time 900 ms has elapsed, the
249 combined dynamics of CTD (according to experimental evidence[6] and
250 prediction from MD simulation, the CTD moves by up to 60 Å; see Extended
251 Data Fig. 12B) and NLD enable HflX to split the 30S from the 50S subunit at
252 the cost of energy set free by GTP hydrolysis and release of the inorganic
253 phosphate (Fig. 4).

254 Given that the combined actions of RRF and EF-G promote ribosome of
255 post-termination ribosomes and that the rate of recycling is comparable to the
256 rate of ribosome splitting by HflX, our observed mechanism of ribosome
257 splitting by HflX can fill in some gaps in explaining details of the general
258 ribosome recycling mechanism.

259

260

261

FIGURES.

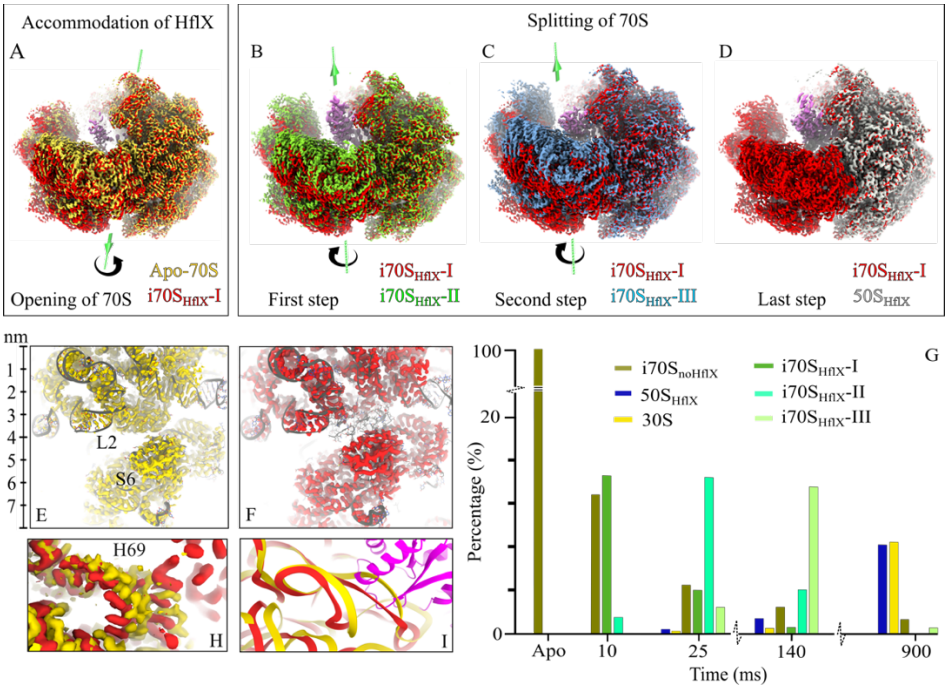

Fig. 1 | Accommodation of HflX on the 70S ribosome and time-dependent 70S splitting: (**A**), Superimposition of reconstructions (Coulomb densities) to show rearrangement of the 30S subunit from apo-70S (yellow) to i70S$_{HflX}$-I (red) to accommodate HflX. The green line represents the initial axis of 30S rotation, Axis I. (**B**) and (**C**), reconstructions of second and third intermediates overlapped with first intermediate, showing the stepwise opening of the 70S by HflX by rotation of the 30S subunit around Axis II (green line). (D), reconstruction of the 50S-HflX complex after the departure of the 30S subunit, overlapped with the first 70S intermediate. In (A) through (D), all reconstructions are aligned on the 50S subunit. (E) and (F), zoomed views of Coulomb densities in yellow for apo-70S and red for i70S$_{HflX}$-I and corresponding atomic models (gray) showing the rearrangement of the intersubunit bridges B7b and B7bR. (**H**) and (**I**), Coulomb densities, and corresponding ribbon models of H69 from apo-70S (yellow), and i70S$_{HflX}$-I (red), respectively, showing the movement of helix H69. HflX is shown in magenta. (**G**) Kinetics of the splitting reaction in terms of the number of particles per class as a function of time, obtained by 3D classification.

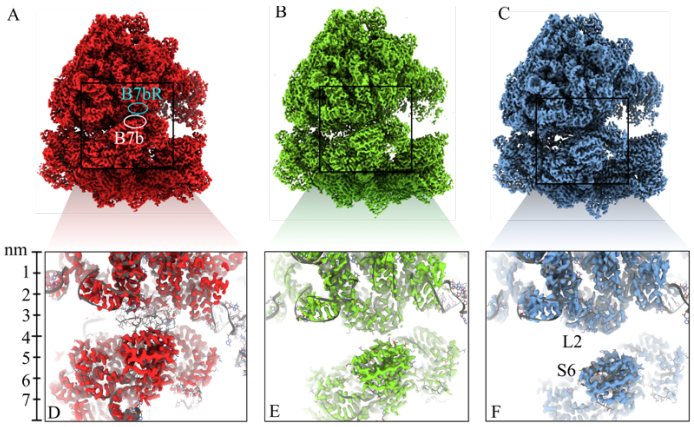

Fig. 2 | Molecular details of subunit interface during the progressive opening of the 70S: (**A**), (**B**), and (**C**), coulomb density maps of intermediates i70S$_{HflX}$-I, i70S$_{HflX}$-II, and i70S$_{HflX}$-III, respectively, in a view showing the separation of the subunits. All maps are aligned on the 50S subunit. (**D**), (**E**), and (**F**), zoomed views showing the time course of splitting of intersubunit bridges B7b and B7bR, and restoration of L2 from disordered (in (**D**) to its original conformation (in (**E**) and (**F**)).

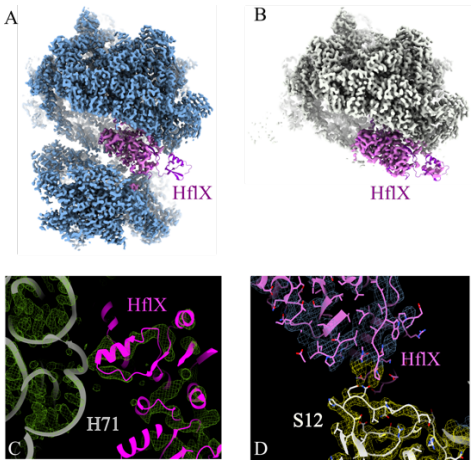

Fig. 3 | Involvement of HflX in 70S splitting. (**A**) Coulomb density of the 70S in i70S$_{HflX}$-III (blue) and associated HflX (magenta) with the fitted atomic model. (**B**) Coulomb density of the final state (gray) showing the 50S subunit with HflX (magenta) along with atomic model. (**C**) Pulling of H71 by the NTD of HflX. (**D**) Pushing of S12 by the HflX GBD flexible loop (E323-G349), leading to dissociation of the 30S subunit from the 70S ribosome.

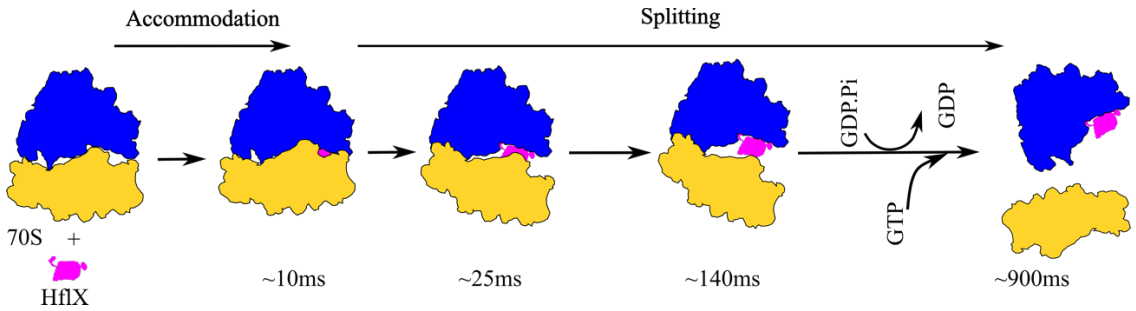

Fig. 4 | Schematic representation of ribosome recycling mechanism. Stepwise splitting of 70S ribosome is shown in the cartoon. The 50S, 30S, and HflX are shown in blue, yellow, and magenta, respectively. The final dissociation of the 30S from 70S occurs after ~140 ms leaving $50S_{HflX}$ as the last state of recycling, where the energy required for a power stroke is set free upon Pi release from GTP·Pi. A new GTP was found to be associated with HflX in the $50S_{HflX}$.

Acknowledgments This work was supported by a grant from the National Institutes of Health R35GM139453 (to J.F.). All data were collected at the Columbia University Cryo-Electron Microscopy Center (CEC). We thank Robert A. Grassucci, Zhening Zhang, and Yen-Hong Kao for their help with the cryo-EM data collection.

Author contributions S.B. conceived the research; S.B., X.F., and J.F. designed the experiments; S.B. prepared the biological samples; X.F. designed the TR chips; S.B. and X.F. performed the TR cryo-EM experiments and data collections; S.B. processed the data; S.M. calculated the subunit and domain motions and the axes of rotation; Z.P.B. helped S.B. with atomic model building and validation, S.B. and J.F. wrote the manuscript with the help of X.F., and S.M. for Methods.

366 **References:**

367

368 1 Zhang, Y. *et al.* HflX is a ribosome-splitting factor rescuing stalled
369 ribosomes under stress conditions. *Nat Struct Mol Biol* **22**, 906-913 (2015).
370 https://doi.org:10.1038/nsmb.3103
371 2 Ngan, J. Y. G. *et al.* HflX is a GTPase that controls hypoxia-induced
372 replication arrest in slow-growing mycobacteria. *Proc Natl Acad Sci U S A*
373 **118** (2021). https://doi.org:10.1073/pnas.2006717118
374 3 Rudra, P., Hurst-Hess, K. R., Cotten, K. L., Partida-Miranda, A. & Ghosh,
375 P. Mycobacterial HflX is a ribosome splitting factor that mediates antibiotic
376 resistance. *Proc Natl Acad Sci U S A* **117**, 629-634 (2020).
377 https://doi.org:10.1073/pnas.1906748117
378 4 Sengupta, S., Mondal, A., Dutta, D. & Parrack, P. HflX protein protects
379 Escherichia coli from manganese stress. *J Biosci* **43**, 1001-1013 (2018).
380 5 Wu, H. *et al.* Structure of the ribosome associating GTPase HflX. *Proteins*
381 **78**, 705-713 (2010). https://doi.org:10.1002/prot.22599
382 6 Coatham, M. L., Brandon, H. E., Fischer, J. J., Schummer, T. & Wieden, H.
383 J. The conserved GTPase HflX is a ribosome splitting factor that binds to the
384 E-site of the bacterial ribosome. *Nucleic Acids Res* **44**, 1952-1961 (2016).
385 https://doi.org:10.1093/nar/gkv1524
386 7 Verstraeten, N., Fauvart, M., Versees, W. & Michiels, J. The universally
387 conserved prokaryotic GTPases. *Microbiol Mol Biol Rev* **75**, 507-542,
388 second and third pages of table of contents (2011).
389 https://doi.org:10.1128/MMBR.00009-11
390 8 Basu, A. & Yap, M. N. Disassembly of the Staphylococcus aureus
391 hibernating 100S ribosome by an evolutionarily conserved GTPase. *Proc*
392 *Natl Acad Sci U S A* **114**, E8165-E8173 (2017).
393 https://doi.org:10.1073/pnas.1709588114
394 9 Blombach, F. *et al.* An HflX-type GTPase from Sulfolobus solfataricus
395 binds to the 50S ribosomal subunit in all nucleotide-bound states. *J Bacteriol*
396 **193**, 2861-2867 (2011). https://doi.org:10.1128/JB.01552-10
397 10 Dey, S., Biswas, C. & Sengupta, J. The universally conserved GTPase HflX
398 is an RNA helicase that restores heat-damaged Escherichia coli ribosomes. *J*
399 *Cell Biol* **217**, 2519-2529 (2018). https://doi.org:10.1083/jcb.201711131
400 11 Adrian, M., Dubochet, J., Lepault, J. & McDowall, A. W. Cryo-electron
401 microscopy of viruses. *Nature* **308**, 32-36 (1984).
402 https://doi.org:10.1038/308032a0

12 Kaledhonkar, S., Fu, Z., White, H. & Frank, J. Time-Resolved Cryo-electron Microscopy Using a Microfluidic Chip. *Methods Mol Biol* **1764**, 59-71 (2018). https://doi.org:10.1007/978-1-4939-7759-8_4

13 Frank, J. Time-resolved cryo-electron microscopy: Recent progress. *J Struct Biol* **200**, 303-306 (2017). https://doi.org:10.1016/j.jsb.2017.06.005

14 Chen, B. *et al.* Structural dynamics of ribosome subunit association studied by mixing-spraying time-resolved cryogenic electron microscopy. *Structure* **23**, 1097-1105 (2015). https://doi.org:10.1016/j.str.2015.04.007

15 Fu, Z. *et al.* Key Intermediates in Ribosome Recycling Visualized by Time-Resolved Cryoelectron Microscopy. *Structure* **24**, 2092-2101 (2016). https://doi.org:10.1016/j.str.2016.09.014

16 Kaledhonkar, S. *et al.* Late steps in bacterial translation initiation visualized using time-resolved cryo-EM. *Nature* **570**, 400-404 (2019). https://doi.org:10.1038/s41586-019-1249-5

17 Hirokawa, G., Iwakura, N., Kaji, A. & Kaji, H. The role of GTP in transient splitting of 70S ribosomes by RRF (ribosome recycling factor) and EF-G (elongation factor G). *Nucleic Acids Res* **36**, 6676-6687 (2008). https://doi.org:10.1093/nar/gkn647

18 Frank, J. & Agrawal, R. K. A ratchet-like inter-subunit reorganization of the ribosome during translocation. *Nature* **406**, 318-322 (2000). https://doi.org:10.1038/35018597

19 Maji, S., Shahoei, R., Schulten, K. & Frank, J. Quantitative Characterization of Domain Motions in Molecular Machines. *J Phys Chem B* **121**, 3747-3756 (2017). https://doi.org:10.1021/acs.jpcb.6b10732

20 Valle, M. *et al.* Locking and unlocking of ribosomal motions. *Cell* **114**, 123-134 (2003). https://doi.org:10.1016/s0092-8674(03)00476-8

21 Ratje, A. H. *et al.* Head swivel on the ribosome facilitates translocation by means of intra-subunit tRNA hybrid sites. *Nature* **468**, 713-716 (2010). https://doi.org:10.1038/nature09547

22 Borovinskaya, M. A. *et al.* Structural basis for aminoglycoside inhibition of bacterial ribosome recycling. *Nat Struct Mol Biol* **14**, 727-732 (2007). https://doi.org:10.1038/nsmb1271

23 Agrawal, R. K. *et al.* Visualization of ribosome-recycling factor on the Escherichia coli 70S ribosome: functional implications. *Proc Natl Acad Sci U S A* **101**, 8900-8905 (2004). https://doi.org:10.1073/pnas.0401904101

24 Dunkle, J. A. *et al.* Structures of the bacterial ribosome in classical and hybrid states of tRNA binding. *Science* **332**, 981-984 (2011). https://doi.org:10.1126/science.1202692